Chelating properties of EDTA-type ligands containing six-membered backbone ring toward copper ion

Cendic, Marina; Deeth, Robert J.; Meetsma, Auke; Garribba, Eugenio; Sanna, Daniele; Matovic, Zoran D.

Published in:
Polyhedron

DOI:
10.1016/j.poly.2016.12.025

Publication date:
2017

Polyhedron 124 (2017) 215–228

Contents lists available at ScienceDirect

Polyhedron

journal homepage: www.elsevier.com/locate/poly

Chelating properties of EDTA-type ligands containing six-membered backbone ring toward copper ion: Structure, EPR and TD-DFT evaluation

Marina Ćendić [a,*], Robert J. Deeth [b], Auke Meetsma [c], Eugenio Garribba [d], Daniele Sanna [e], Zoran D. Matović [a,*]

[a] University of Kragujevac, Faculty of Science, Department of Chemistry, Radoja Domanovića 12, 34000 Kragujevac, Serbia
[b] Department of Chemistry, Inorganic Computational Chemistry Group, University of Warwick, Coventry CV4 7AL, UK
[c] Stratingh Institute for Chemistry and Chemical Engineering, University of Groningen, Nijenborgh 4, NL-9747 AG Groningen, Netherlands
[d] Dipartimento di Chimica e Farmacia, Università di Sassari, Via Vienna 2, I-07100 Sassari, Italy
[e] Istituto CNR di Chimica Biomolecolare, Trav. La Crucca 3, I-07040 Sassari, Italy

ARTICLE INFO

Article history:
Received 25 October 2016
Accepted 18 December 2016
Available online 28 December 2016

Keywords:
Copper(II)–aminopolycarboxylates
Syntheses
LFMM
EPR
TD-DFT

ABSTRACT

The P-APC ligands (EDTA-like aminopolycarboxylate ligands comprising 1,3-propanediamine backbone) H_4pdta, H_4pd3ap, H_4pddadp and H_4pdtp (H_4pdta = 1,3-propanediamine-*N*,*N*,*N*′,*N*′-tetraacetatic acid; H_4pd3ap = 1,3-propanediamine-*N*,*N*,*N*′-triacetic-*N*′-3-propionic acid; H_4pddadp = 1,3-propanediamine-*N*,*N*′-diacetatic-*N*,*N*′-di-3-propionic acid; H_4pdtp = 1,3-propanediaminetetra-3-propionic acid) were investigated. The chelating ligands coordinate to copper(II) via five or six donor atoms affording distorted trigonal-bipyramid and octahedral structures that were verified by X-ray analysis for Ba[Cu(pd3ap)]·$6H_2O$ (**1**) and *trans*(O_6)-Ba[Cu(pddadp)]·$8H_2O$ (**2**) complexes respectively. The impact of counter-ions on the P-APC complexes is shown in detail together with the analysis of another strain parameters. EPR spectral results confirm the penta-coordination of **1** and hexa-coordination of **2** in aqueous solution, even if several Cu(II) species with different protonation degree exist as a function of pH, and indicate that a hexa-coordinated structure is favored when the two axial COO^- donors close five-membered chelate rings. We also present here the results of molecular mechanics (LFMM) calculations based on our previously-developed force field along with results of DFT (Density Functional Theory). On the basis of extensive DFT and TD-DFT calculations the B1LYP/6-311++G(d,p) level has been seen as an accurate theory for calculating and predicting the UV–Vis spectra in case of copper–P-APC compounds.

1. Introduction

EDTA-like aminopolycarboxylate ligands have a remarkable ability to chelate transition metal ions. The most typical applications lie in: metal detoxification [1], treatment of HIV infection [2], diagnostic X-ray and magnetic resonance imaging [3] etc. Our interest in APC ligands concerns their potential medicinal use in the treatment of neural disorders (Wilson's and Alzheimer's disease) [4]. We are investigating influence of EDTA-like ligands on homeostasis of copper ion; so far we have obtained promising results from *in vivo* tests (the copper level has been monitored in the experimental rats treated with APCs) which indicate that EDTA-like ligands containing mixed carboxylate arms most dramatically inactivate copper ions (presumably copper(II) ion however not excluding copper(I)). Accordingly, it is of major importance to explore behavior of the copper(II) state with structurally different EDTA-like chelate molecules. Recently, we reported copper(II) complexes of E-APCs (EDTA-like aminopolycarboxylate ligands comprising ethylenediamine backbone) using structure [5] and theory [6] as a basis for research. In this paper, we combine both studies on a set of Cu(II)–P-APC (comprised 1,3-propanediamine backbone) complexes. A part of the present research (EPR based) includes both P-APC and E-APC classes of complexes with various combinations of acetate and propionate arms (Fig. 1). Thus, H_4eddadp (ethylenediamine-*N*,*N*′-diacetic-*N*,*N*′-dipropionic acid), $H_4$1,3-pddadp (1,3-propylenediamine-*N*,*N*′-diacetic-*N*,*N*′-dipropionic acid) are of potential interest. Although their copper(II) complexes have somewhat weaker stability constants than Cu(II)-edta, the work of Chaberek and co-workers [7] suggests that they are more selective toward the Cu(II) ion compared to other metals. However, it was clear that the acetate groups form more stable chelate structures than do β-propionate

* Corresponding authors.
E-mail addresses: marina.cendic@kg.ac.rs (M. Ćendić), zmatovic@kg.ac.rs (Z.D. Matović).

http://dx.doi.org/10.1016/j.poly.2016.12.025
0277-5387/

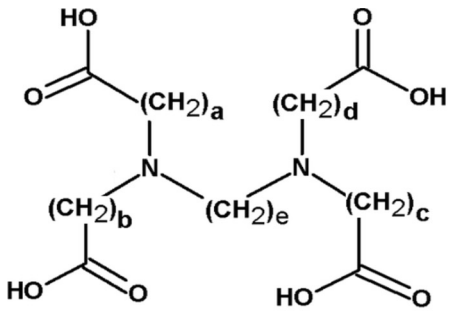

pro-ligand	a	b	c	d	e	No 6-membered rings
H_4edta	1	1	1	1	2	0
H_4edtp	2	2	2	2	2	4
H_4pdta	1	1	1	1	3	1
H_4pd3ap	2	1	1	1	3	2
H_4pddadp	2	2	1	1	3	3
H_4pdtp	2	2	2	2	3	5

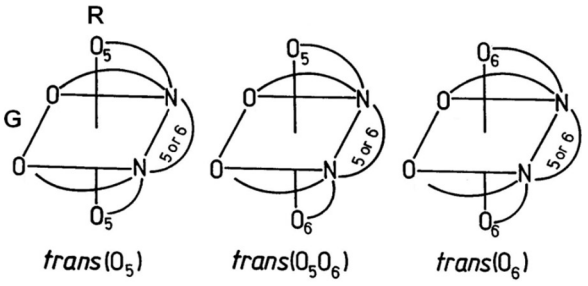

Fig. 1. The general structure of APCs and geometrical isomerism of six-coordinate $[M(edta\text{-}type)]^{n-}$ complexes. The *trans*(*On*) nomenclature refers to the size of the carboxylate chelate rings for the oxygen donors; G stands for equatorial plane and R stands for axial line.

groups ($H_4$1,3-pdta = 18.92 [8]; H_4eddadp = 16.3 [8]; $H_4$1,3-pddadp = 14.96 [8]) which gives a chance to $H_4$1,3-pdta (1,3-propylenediaminetetracetic acid) chelate holding 1,3-propanediamine backbone to be effective in copper immobilization. In support of this, Deeth and co-workers [6] demonstrated that LFMM also gives a smooth correlation between stability constant and the number of six-membered chelate rings with log β decrease as the number of six-membered rings increase.

Two or three geometrical isomers are possible for APCs with different lengths of carboxylate arms: *trans*(O_5), *trans*(O_5O_6) and *trans* (O_6) (O_5 and O_6 stands for five- and six-membered carboxylate arms) (Fig. 1). For the H_4pddadp, all three isomers of $[Cr(pddadp)]^-$ complex [9] were isolated. The octahedral P-APC complex $[Cu(pdta)]^{2-}$ [10] has been prepared with $pdta^{4-}$ acting as hexadentate. There are no preparative and structural data for H_4pd3ap and H_4pdtp ligands and their corresponding copper(II) complexes. We also attempt to investigate the nature of solution and solid state influence, monitoring the level of axial or equatorial distortion. With this idea in mind, we prepared an additional $[Cu(pddadp)]^{2-}$ complex anion bearing Ba^{2+} as a counter-ion. The Ba^{2+} complex is placed along with Na^+ and H^+ (physiologically present in the body fluids) complexes and a comparative structural study has been made. The computational study has been undertaken using different DFT methods and basis sets with an aim to establish the best approach with respect to the energy and geometry of the complexes. The DFT calculations are compared with a recently developed LFMM force field [6] implemented in the molecular operating environment (MOE) [11]. To be able to calculate, predict and monitor spectral parameters of complexes the details of the comprehensive TD-DFT analyses are given as well. Finally, we would like to clarify P-APCs/copper interactions by general correlation of their solution, electronic and structural properties.

2. Experimental

2.1. Materials and measurements

Reagent-grade, commercially available chemicals were used without further purification. The 1,3-propanediamine, 3-chloropropionic and chloroacetic acids were purchased from Fluka and used as supplied. The $Ba[Cu(edta)]\cdot 6H_2O$ [12], $K_2[Cu(edtp)]\cdot 4H_2O$ [13] and $Mg[Cu(pdta)]\cdot 8H_2O$ [10] were prepared according to procedures given elsewhere.

2.2. Synthesis of ligands and complexes

2.2.1. Preparation of (1,3-propanediamine-N,N,N′-triacetic-N′-3-propionic) acid, H_4pd3ap (Condensation mixture)

Solution A Monochloroacetic acid (11.50 g, 120 mmol) was dissolved in 42 ml of demineralized water and 4.70 g (84 mmol) of calcium oxide was added to the solution. The pH rose from 1.0 to 11.2. Subsequently, 3.11 g (42 mmol) of 1,3-propanediamine was added within 10 min. The temperature was kept at about 50 °C without additional heating. After 1 h the temperature was increased to 70 °C and the resulting mixture was left for an additional 5.5 h. During the entire reaction the pH was kept constant at 7.5–8.0 by the addition of calcium oxide. At the end of the reaction, a total of 1.90 g (34 mmol) of calcium oxide was added. The reaction mixture was filtered warm over a glass filter to remove the excess of calcium hydroxide. The reaction mixture (volume 50 ml) contains H_3pd3a (50%), H_4pdta (18%) and H_2pdda (23%) ligands. This was checked by means of chromatography of copper (II) complexes within the above mixture. To the reaction mixture a solution of 9.44 g (236 mmol) NaOH in 15 ml of water was added. The deposited $Ca(OH)_2$ was separated by filtration under vacuum; *Solution B*: A solution obtained by dissolving 4.53 g (42 mmol) of 3-chloropropionic acid in 10 ml of water was cooled in an ice bath and carefully neutralized with a cold solution of 1.68 g NaOH (42 mmol) in 5 ml of water, making sure that the solution temperature did not exceed 15 °C; The *Solution B* was then added to *Solution A* (pH ~ 7.5). The reaction mixture was gradually warmed up with stirring to 55 °C during 5 h (where pH was maintained at ~8 by NaOH (1.68 g, 42 mmol in 5 ml of water). The volume of solution was held on 50 ml.

2.2.2. Preparation of barium(1,3-propanediamine-N,N,N′-triacetato-N′-3-propionato) cuprate(II) hexahydrate, $Ba[Cu(pd3ap)]\cdot 6H_2O$ (**1**)

A 6.84 g (42 mmol) amount of $CuCl_2\cdot 2H_2O$ was dissolved in 15 ml of water and was added to equivalent amounts of the mixture of P-ACP acids described above with mixing and heating at 65 °C for one hour. In order to keep the pH at 7, a solution of

$NaHCO_3$ was added in small portions. The volume was maintained by the addition of hot water. The blue colored synthesized mixture was then filtered. The filtrate was then evaporated to a small volume and desalted by the technique of gel-filtration (Sephadex G-10 was used in this purpose). The resulting blue solution was poured into a 5 × 60 cm column containing a Dowex 1-X8 (200–400 mesh) anion-exchange resin in the Cl^- form. The column was then washed with water and eluted with a 0.1 M solution of $BaCl_2$. Three bands were obtained. The eluates were evaporated to a small volume and desalted by passage through a G-10 Sephadex column, with distilled water as the eluent. The first and third eluate corresponds to $[Cu(pddadp)]^{2-}$ and $[Cu(pdta)]^{2-}$ complexes respectively. The second eluate was concentrated to a volume of 3 ml and stored in a desiccator over ethanol for several days. The blue crystals were collected and air-dried. Yield: 5.1 g (19.5%) of Ba[Cu(pd3ap)]·$6H_2O$. Elemental analysis is consistent with the composition of Ba[Cu(pd3ap)]·$6H_2O$: $C_{12}H_{28}N_2O_{14}CuBa$, Mw = 625.23. Anal. Calc.: C, 23.05; H, 4.51; N, 4.48. Found: C, 23.26; H, 4.54; N, 4.50%. Melting point: 217 °C.

2.2.3. Preparation of the trans(O_6) isomer of barium(1,3-propanediamine-N,N′-diacetato-N,N′-di-3-propionato) cuprate(II) octahydrate, Ba[Cu(pddadp)]·$8H_2O$ (**2**)

This complex was prepared by a previously described procedure [14], using $BaCl_2$ as an eluent for anion chromatography. Blue crystals of Ba[Cu(pddadp)]·$8H_2O$ were obtained. Elemental analysis is consistent with the composition of Ba[Cu(pddadp)]·$8H_2O$: $C_{13}H_{34}N_2O_{16}CuBa$, Mw = 675.29. Anal. Calc.: C, 23.12; H, 5.07; N, 4.15. Found: C, 23.08; H, 4.98; N, 4.20%. Melting point: 234 °C.

2.2.4. Preparation of (1,3-propanediamine-N,N,N′N′-tetra-3-propionic) acid, H_4pdtp (Condensation mixture)

The solution obtained by dissolving 3-chloropropionic acid (23.87 g, 200 mmol) in 50 ml of water was cooled in an ice bath and carefully neutralized with cold sodium hydroxide, NaOH (8.00 g, 200 mmol in 20 ml of water) ensuring that the temperature did not exceed 5 °C. With this solution the required amount of 1.3-propanediamine (3.00 g, 40 mmol, 3.38 ml) was then added. The entire reaction mixture was heated to a temperature of 50 °C, with stirring, followed by gradual addition of sodium hydroxide, NaOH (8.00 g, 200 mmol in 20 ml of water) controlling the pH in the range 7–8 over two days.

2.2.5. Preparation of barium(1,3-propanediamine-N,N,N′N′-tetra-3-propionato)cuprate(II)trihydrate, Ba[Cu(pdtp)]·$3H_2O$ (**3**)

To the condensation mixture containing H_4pdtp acid (40 mmol, 50 ml) was added $CuCl_2·2H_2O$ (6.80 g, 40 mmol). A solution of dark blue color was obtained. The pH was adjusted with sodium hydroxide to 7–8. The solution was heated for 1 h at 65–70 °C and strained from NaCl. The filtrate was then evaporated to a small volume and desalted by the technique of gel-filtration (Sephadex G-10). The resulting blue solution was poured into a 5 × 60 cm column containing a Dowex 1-X8 (200–400 mesh) anion-exchange resin in the Cl^- form. The column was then washed with water and eluted with a 0.05 M solution of $BaCl_2$. Two bands were obtained. The second dark blue eluate was evaporated to a small volume and desalted by passage through a G-10 Sephadex column, with distilled water as the eluent. The eluate was concentrated to a small volume and stored in a desiccator over ethanol for several days. The light blue powder was collected. Yield: 7.38 g (30%) of Ba[Cu(pdtp)]·$3H_2O$. Elemental analysis is consistent with the composition of Ba[Cu(pdtp)]·$3H_2O$: $C_{15}H_{28}N_2O_{11}CuBa$, Mw = 613.26. Anal. Calc. for the complex salt: C, 31.64; H, 5.09; N, 6.15. Found: C, 31.54; H, 5.20; N, 6.04%. Melting point: 206 °C.

2.3. Physical measurements

Block shaped, light blue (1) and green-blue (2) colored, crystals were obtained by recrystallization from water. A crystal with the dimensions of 0.45 × 0.19 × 0.12 mm (1) and 0.31 × 0.21 × 0.17 mm (2) was mounted on top of a glass fiber and aligned on a Bruker [15] SMART APEX CCD diffractometer (Platform with full three-circle goniometer). The crystals (1) and (2) were cooled to 100(1) K. Intensity measurements were performed using graphite monochromated Mo-K radiation from a sealed ceramic diffraction tube (SIEMENS). The final unit cell was obtained from the *xyz* centroids of 6710 (1) and 8046 (2) reflections after integration. The structure was solved by Patterson methods and extension of the models was accomplished by direct methods applied to difference structure factors using the program DIRDIF [16]. Final refinement on F_o^2 was carried out by full-matrix least-squares techniques. Crystallographic and experimental details of the structures are summarized in S1 and S2 in the Supporting information.

Anisotropic EPR spectra were recorded from 2000 to 4000 G at 120 K with an X-band (9.4 GHz) Bruker EMX spectrometer equipped with an HP 53150A microwave frequency counter. The concentration of Cu(II) complexes used to record EPR spectra in aqueous solution was 1×10^{-3} M and the solutions were obtained dissolving polycrystalline samples in water. EPR spectra on the solid polycrystalline compounds were recorded at 77 K. The modulation frequency was 100 kHz and modulation amplitude was 4 Gauss.

IR spectra in the 400–4000 cm^{-1} region were recorded on a Perkin Elmer FTIR spectrophotometer SpectrumOne, using the KBr pellets technique. Electronic absorption spectra were recorded on a Perkin Elmer Lambda 35 spectrophotometer. For these measurements 1×10^{-2} M aqueous solutions (pH ~ 7) of the complexes under investigation were used.

C, H, N analyses were performed at the Microanalytical laboratory, Faculty of Chemistry, University of Belgrade, Serbia. Melting points were measured by a Stuart melting device with accuracy ±1 °C.

2.4. Computational details

Part of DFT calculations used the Amsterdam Density Functional code version ADF2012 [17–19]. Details on ADF calculation procedure are given in S3 of Supporting information. The GAUSSIAN09 program [20] has been used for running DFT part as well. For these calculations, we used the unrestricted BP86 and/or B3LYP and/or B1LYP hybrid functional and Ahlrich's def2-TZVP [21] or 6-311++G(d)(p) [22] basis sets. The TD-DFT method required special treatment: all structures were optimized by using the 6-311++G(d)(p) basis set for all atoms; the solvation was also incorporated by performing the TD-DFT calculations in the presence of a self-consistent reaction field (SCRF) by using the polarizable continuum models (PCM); the 3 XC functional investigated can be divided into two categories: (i) pure GGA functional BP86 and (ii) hybrid GGA functional including B1LYP and B3LYP [20]. For simulation of TD-DFT spectra (with $\Delta_{1/2,I} = 3000\ cm^{-1}$) we used AOmix 6.87 software [23]. LFMM calculations [24] employed the extended version of MOE version 2013.0801. The LFMM and MMFF94 force field parameters were as described previously. To assist with the correct description of six-membered Cu-propanediamine chelate rings, a Cu–N torsional restraint was added as described elsewhere [25].

3. Results and discussion

P-APCs with an N2O4 chromophore containing five- and/or six-membered carboxylate arms (Fig. 2): H_4pdta, H_4pd3ap, H_4pddadp

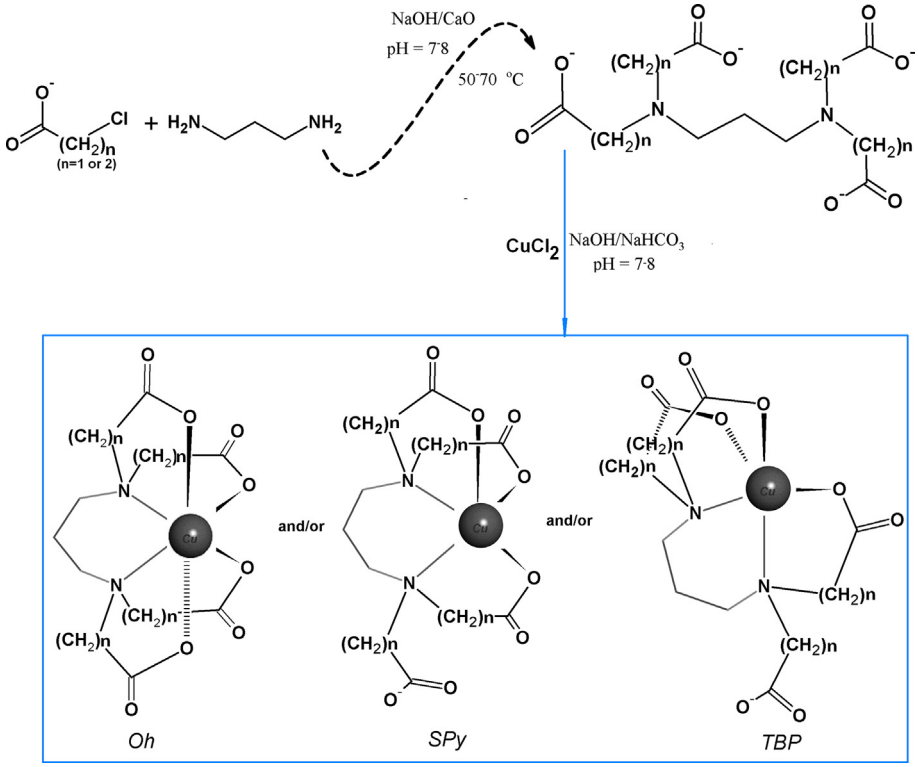

Fig. 2. Synthesis of the $[Cu(II)(P\text{-}APCs)]^{n-}$ complexes.

and H_4pdtp have been used for complexation of copper(II) ion. The P-APC synthesis has followed several methods: (i) condensation starting from neutralized α- or β-monohalogencarboxylic acid and the corresponding diamine; (ii) condensation of acrylic acid and diamine, and (iii) condensation of dihalogen derivatives of diamine with diverse amino-acids. Here the hexadentate P-APCs have been prepared either as a condensation mixture or pure acid starting from neutralized α or β chloro-aliphatic acid and 1,3-propanediamine.

Depending on the structure of the P-APC ligands, the pentadentate form can be expected, as is the case of the trigonal-bipyramidal $[Cu(pd3ap)]^{2-}$ complex, or hexadentate with symmetrical H_4pdta, H_4pddadp and H_4pdtp ligands (octahedral coordination). Structural variations of the P-APC's framework involve increasing the size of the backbone and/or carboxylate rings to generate less strained systems. Geometrical isomerism is possible for complexes of the P-APCs where the carboxylate arms are replaced so as to form chelate rings of different size (Fig. 1). In the case of H_4pd3ap, a mixture of pentadentate and hexadentate $[Cu(pd3ap)]^{2-}$ complexes was formed. Therefore, there is a delicate balance between geometries as shown in Fig. 2. This depends on many factors such as: the structure of the P-APC ligand, pH (see later on) and the nature of counter-ion. We have isolated, by means of chromatography, a pentadentate form of $[Cu(pd3ap)]^{2-}$ complex with one six-membered chelate ring, detached from the copper (TBP geometry). By the same method, octahedral $[Cu(pdtp)]^{2-}$ has been prepared as well. All the substances in this study were fully characterized by all available methods (NMR, IR, EPR, UV–Vis etc.). The structures of two prepared complexes **(1)** and **(2)** were verified by X-ray analysis.

3.1. Structural parameters of (1) and (2)

A structural diagram of the $[Cu(pd3ap)]^{2-}$ anion, with its adopted atom-numbering scheme is shown in Fig. 3. The asymmetric unit consists of eight moieties: a Ba^{2+} cation, $[Cu(pd3ap)]^{2-}$ anion and six solvent water molecules with no atom sitting at a special position.

Detailed analysis of the structures is presented in the Supporting information. The triclinic unit cell contains two asymmetric units, meaning two cations, two anions and twelve water molecules (Fig. 3). The $pd3ap^{4-}$ anion acts as a pentadentate chelate with one detached axial arm forming a TBP complex. The Cu–L distances range from 1.9329(17) to 2.1269(18) Å (see Table S1 in the Supporting information) and are comparable with those in related Cu(APC)-type complexes [26]. An axial Cu–O bond value (Cu2–O25 = 2.1269(18) Å) is slightly shorter than found in a similar square-pyramidal $[Cu(pd3a)]^{-}$ complex anion (Cu–O = 2.18; 2.23 Å) [27]. The six-membered backbone 1,3-propanediamine ring has a half-chair conformation while in- and out of plane (G) acetate rings have twisted conformations. The trigonal-based five-membered chelate ring also adopts a twisted form. The fact that one β-alaninato ring is detached results in a distorted TBP geometry and therefore the accompanying asymmetry in the axial bond distances could be due to the steric demands of the in-plane coordinated acetate ring or as a consequence of the high stability of copper(II)–N_2O_3 chromophore already seen in the $[Cu(pd3a)]^{-}$ complex. Recently, we observed that the more six-membered rings, the more pronounced the trigonality [27]. The trigonality τ (angular structural parameter is defined and proposed as an index of trigonality, as a general descriptor of five-co-ordinate centric molecules [28]) for the $[Cu(pd3ap)]^{2-}$ complex of 73% indicates that this structure has a distorted TBP geometry. A structural diagram of the *trans*(O_6)-$[Cu(pddadp)]^{2-}$ complex is also shown in Fig. 2. Each asymmetric unit contains one formula unit, consisting of ten moieties: the Ba^{2+} cation, $[Cu(pd3ap)]^{2-}$ anion and eight solvate water molecules. The triclinic unit cell contains twenty units, two cations, two anions and sixteen water moieties. The anion $pddadp^{4-}$ (Fig. 4a) acts as a hexadentate ligand with six coordinated bonds forming a distorted octahedral complex. The Cu–L

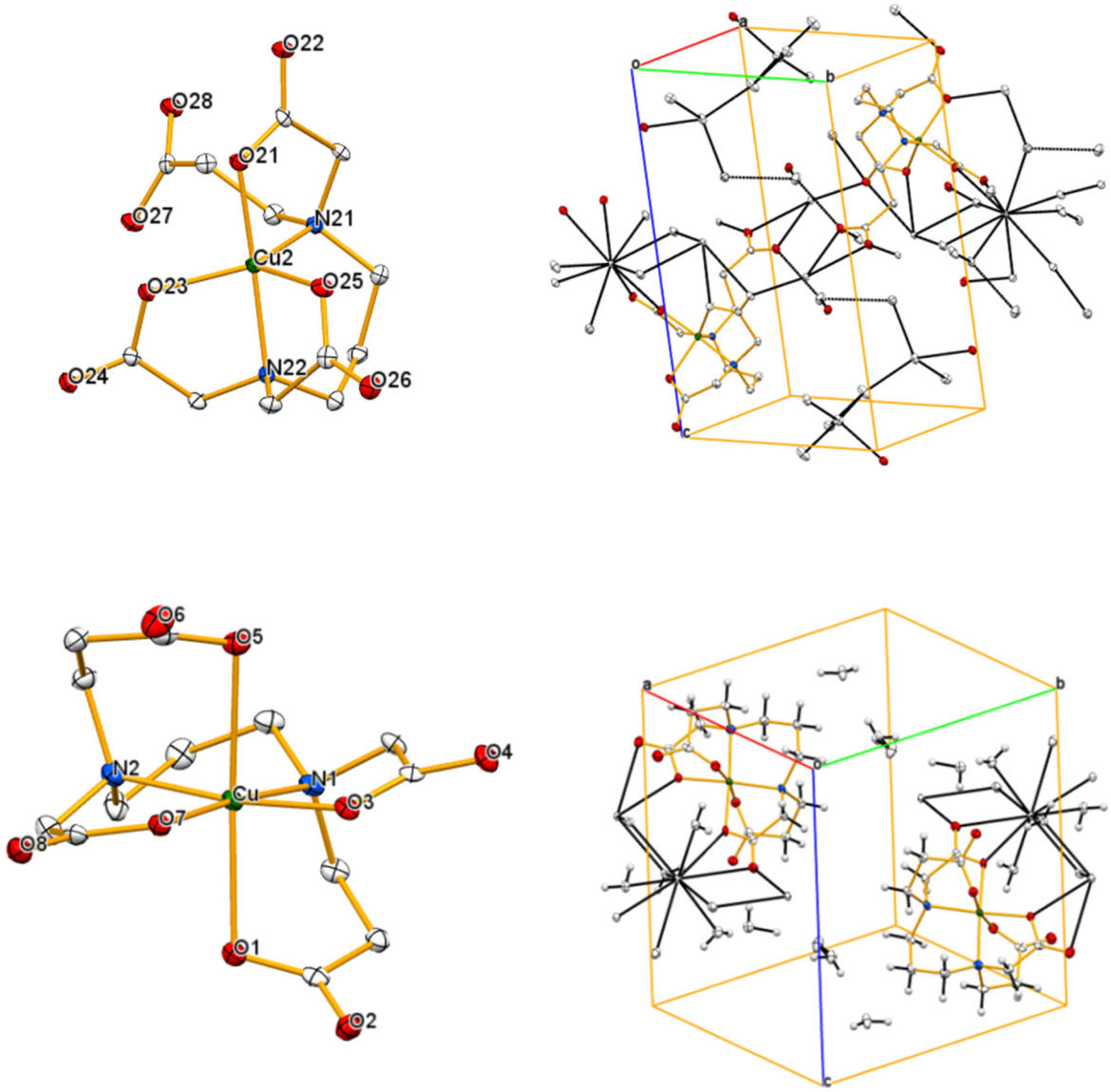

Fig. 3. Above: X-ray crystal structure of $[Cu(pd3ap)]^{2-}$ anion and crystal packing along the *a* axis showing hydrogen bonds; below: X-ray crystal structure of *trans*(O_6)-$[Cu(pddadp)]^{2-}$ anion and crystal packing along the *a* axis. Hydrogen atoms are omitted because of clarity.

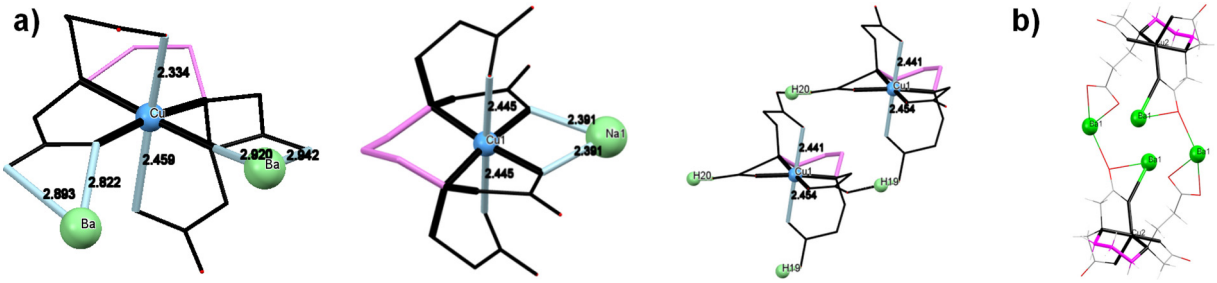

Fig. 4. (a) Ba^{2+}, Na^{+} and H^{+} counter ions in the case of $[Cu(pddadp)]^{2-}$ complex; (b) X-ray defined structure of Ba[Cu(pd3ap)] dimmer.

distances range from 1.971(2) to 2.459(2) Å (see Table S2 in the Supporting information) are comparable to related copper(II)–APC systems [26]. There are two longer asymmetric axial bonds (Cu–O1 = 2.334(2)) and Cu–O5 = 2.459(2)). The six-membered backbone 1,3-propanediamine ring has a boat conformation, the in-plane (G) acetate rings have quasi planar conformations, and the axial chelate ring (R) adopts a slightly twisted boat form.

3.2. Copper–P-APC geometry dependence with respect to the structure of the ligand, geometry of the complex and the nature of counter-ions

To analyze Cu(II)–P-APC strain in more details the following four terms should be considered: (a) the *cis* and *trans* angles around the central ion; (b) the ring angle sums of the various kinds of rings; (c) the Cu–O–C or Cu–N–C bond angles; (d) the bond

angles that a coordinated N atom makes with its connectors. The structural data correlating the stereochemistry of the Cu(II) complexes are given in Table 1. These data provide the basis for the detailed analysis of the impact of counter-ions on the structure and stereochemistry of the $[Cu(pddadp)]^{2-}$ complex. In the case of the quasi-symmetric $[Cu(pddadp)]^{2-}$ complex ion we compared the influence of Na^+, Ba^{2+} and H^+ counter ions. Different ions lead to changes in strain parameters of the P-APC systems (Table 1). The $\Sigma\Delta(O_h)$ parameter (the sum of the absolute values of the deviations from 90° of the L–M–L′ bite angles) for all hexadentate complexes is similar. In case of $\Sigma\Delta$(Ring) strain parameter (the deviation from the ideal of the corresponding chelate rings bond angle sum) the situation is different. The $\Delta\Sigma$ (Ring R) values vary from +7 in case of Ba^{2+} complex to +25 for the H^+ complex (blue column). The Cu–O–C fragment of the carboxylate rings is expected to attain a bond angle between 109.5° and 120° depending on the degree of covalency of the M–O bond. The Cu–O–C bond angles of the elongated copper(II) chelates should deviate minimally when there are no 3-propionato rings (this was demonstrated for the Cu–E–APCs [1]). The Cu–O–C angles for the axial β-alaninato rings of the elongated Cu(II)–pddadp (with Ba^{2+}, Na^+ and H^+ cations) deviate minimally from the ideal bond angle of 109.5°. In the complex with the Ba^{2+} cation this deviation is negative (−5°) and for the Na^+ and H^+ complexes it is positive and varies from 0 to +5° (blue column). The total deviation around N atoms (Table 1) sums to roughly 13° and 17° for Ba^{2+} and Na^+ complexes, respectively, and the greatest deviation (20°) was found for the H^+ complex (blue column). The extent of distortion is restricted by chelation of the multidentate ligand and depends on its structure as well as the geometry of the complex. Owing to the presence of the Jahn–Teller effect (ligand field stabilization), the APCs preferentially coordinates in an equatorial plane and such a coordination can produce the tetragonally elongated octahedral complexes. The geometry depends on the in-plane ligand field strength, the structure of the ligand and the size of its chelate rings. The tetragonality parameter T (taken as the ratio of the average equatorial Cu–O bond lengths to the average axial Cu–O bond lengths with values typically around 0.8 ± 0.02) [29] decreases in the order: $Ba^{2+} > Na^+ \geqslant H^+$ complexes (Table 1). The same values have been obtained for tetragonal octahedral complexes [30,31]. We observed that the variation in tetragonality and axial Cu–O bond asymmetry (Table 1) depends on the nature of the counter-ion and its covalent interaction with the coordinated carboxylate groups. The Ba^{2+} complex prepared in this work shows moderate distortion (T = 0.823). The Jahn–Teller effect is most pronounced for the more distorted Na^+ (T = 0.799) and H^+ complex (T = 0.798). In the case of quasi symmetrical complexes such as $[Cu(pddadp)]^{2-}$, the asymmetry of axial O–Cu–O bonds arises not only from intramolecular bonding but primarily from covalent/electrostatic interactions of counter-ion and complex anion. The asymmetry in bonding of the Ba^{2+} cation with equatorial oxygen pairs (Fig. 4) results in the asymmetric strengthening of axial Cu–O bonds (2.459 and 2.334 Å).

The interaction of Ba^{2+} with the first carboxylate oxygens (2.822 Å) lowers the strength of the matching nitrogen and oxygen in the equatorial field and amplifies the bonding effect of the corresponding axial oxygen (shortened length of 2.334 Å) (Fig. 4a). Changing the direction of bonding toward the second oxygen pair results in the opposite effect (longer length of 2.459 Å). The quasi symmetrical structures of Na^+ and H^+ complexes derive from balanced electrostatic and covalent influences of Na^+ and H^+ ions (Fig. 4a). The observed symmetry of the crystal packing unit in the Na^+ complex is a result of the absence of any hydrogen bonds and other short contacts. The sodium ion acts symmetrically on both equatorial rings which leads to the equal strengthening on the axial field resulting in equal axial Cu–O bonds of 2.445 Å.

The hydrogen bonds of the H^+ complex are, on the whole, symmetrical (Fig. 4a) in the sense that there is an identical influence of hydrogen bonds and atoms in the equatorial and axial positions and, accordingly, the regular elongated octahedral geometry was reported. Finally, the impact of counter-ions to the complex geometry can be of primary or secondary importance. When the influence of ions on the equatorial or axial plane is too strong, like in the Ba^{2+} complex, the axial bond of the six-membered ring already lengthened by the presence of a five-member ring in equatorial plane is further weakened by the strong influence of the Ba^{2+} ion in the G plane. One may conclude that the nature of the counter-ion may have an impact on the complex configuration; in this case it is reflected through asymmetric bond lengths.

The strain parameters of $[Cu(pd3ap)]^{2-}$ (Table 1) derived from DFT optimized *trans*(O_5) and *trans*(O_5O_6) isomers were compared with strain values of the experimental TBP $[Cu(pd3ap)]^{2-}$ complex. The *trans*(O_5O_6) geometrical isomer does not show large deviations (Table 1) which should relate to the relative stability of this isomer in solution. However, the *trans*(O_5) isomer shows a difference, primarily in the β-alaninato ring ($\Delta\Sigma$(Ring G) = +31 and Δ(Cu–O–C) (Ring R) = +17 (yellow columns in Table 1). This causes the large in plane deviation of the *trans*(O_5) six-membered ring (DFT gives an advantage to *trans*(O_5O_6) isomer with energy difference of 1.21 kcal/mol). Therefore, the *trans*(O_5O_6) isomer has been seen

Table 1
Strain analysis of copper complexes with 1,3-propanediamine ligands with five- and six-membered carboxylate rings (see Ref. [32]).

Complex	$\Sigma\Delta(O_h)$[a]	T	$\Delta\Sigma$(ring)[b] R	$\Delta\Sigma$(ring)[b] G	Δ(Cu–O–C)[c] R	Δ(Cu–O–C)[c] G	$\Sigma\Delta$(N)[d]	T[e]	Ref.
trans(O_6)-Ba[Cu(pddadp)]	51	+27	+7	−9	−5	+4	13	0.823	This work
trans(O_6)-Na_2[Cu(pddadp)]	43	+27	+14	−11	0	+5	17	0.799	[14]
trans(O_6)-H_2[Cu(pddadp)]	44	+23	+25	−11	+5	+4	20	0.798	[32]
trans(O_5O_6)-Ba[Cu(pd3ap)][f]	51	+26	+5(0)	−12	−6(+1)	+3	16	0.839	This work
trans(O_5)-Ba[Cu(pd3ap)][f]	66	+23	0	+31(−18)	+2	+17(+3)	17(16)	0.870	This work
[Cu(pd3ap)][g]	91	+33	−20	−10	+2	+5	20	0.924	This work

[a] $\Sigma\Delta(O_h)$ is the sum of the absolute values of the deviations from 90° of the L–M–L′ bite angles. All values rounded off to the nearest degree.
[b] $\Delta\Sigma$(ring) is the deviation from the ideal of the corresponding chelate rings' bond angle sum.
[c] Δ(Cu–O–C) (ring) is the mean value of the deviation of the corresponding rings' Cu–O–C bond angle from the 109.5°.
[d] $\Sigma\Delta$(N) is the sum of the absolute values of the deviations from 109.5° of the six bond angles made by nitrogen atoms. A mean value for the two nitrogens is reported.
[e] Tetragonality, expressed as ratio of mid-length in plane and medium-length in the axial position.
[f] DFT structures: LDA/DZP.
[g] TBP complex (X-ray crystal structure).

as a molecule potentially found in solution, and therefore potentially being able to be converted. We are of the opinion that divalent barium counter ion play not only charging and solid state cell packing role but also may contribute to the substantial change of the complex geometry. One may see that barium cations (Fig. 4b) pull down along axial O–Cu–O axes G acetate ring and, therefore, contribute to detaching of β-propionate oxygen by synchronized effects of $Ba^{2+}\cdots{}^{-}OOC$ attraction and steric overcrowding.

3.3. Spectroscopy

3.3.1. EPR of APCs

In agreement with previously reported data [33], edta forms with Cu(II) ion two complexes, the first at acid pH values (pH < 4) with (2 N, 3 COO^-) coordination (g_z 2.330, A_z 154.6×10^{-4} cm^{-1}, **I** in Fig. 5 (1)) and the second one from pH 4 with (2 N, 4 COO^-) coordination (g_z 2.292, A_z 160.5×10^{-4} cm^{-1}, **II** in Fig. 5 (1)). All the EPR parameters are reported in Table 2.

H_4edtp forms (6,5,6)-chelate rings in the equatorial plane. Square pyramidal coordination (2 N, 3 COO^-) has been established in the solid state. The same coordination is retained in solution. EPR parameters, g_z 2.287, A_z 168.5×10^{-4} cm^{-1} (**I** in Fig. 5 (2)), are very similar to those of the species with (2 N, 4 COO^-) coordination formed by pdta for which (5,6,5)-chelate rings are closed in the equatorial plane. In contrast to the edta complex, on the basis of the EPR parameters (g_z 2.283, A_z 165.1×10^{-4} cm^{-1}, **I** in Fig. 5 (3)), the H_4pdta forms only one species in the pH range 3–10 with (2 N, 4 COO^-) coordination, which is in agreement with the X-ray crystal structure of $[Cu(pdta)]^{2-}$ [10]. Comparing the spectroscopic data measured for H_4edta and H_4pdta it is possible to observe a slight decrease of g_z and a slight increase of A_z in agreement with a more relaxed structure due to the larger size of the chelate ring formed by the two nitrogen donors (six- *vs*. five-membered *N*,*N* chelate ring) [34]. Increasing the size of the central ring from (5,5,5)-chelation for H_4edta to (5,6,5)-chelation for H_4pdta (the two axial position are occupied by COO^- groups) a slight decrease of g_z and an increase of A_z is expected [34], in agreement with what is observed experimentally. A good parameter which measures the distortion degree of the equatorial plane of a Cu(II) species is the ratio g_z/A_z [35] and it is 106 for a complex with a high degree of planarity such as $[Cu(GlyGlyGlyGlyH_{-3})]^{2-}$ with (NH_2, N^-, N^-, N) coordination [34] and 143 and 138 for the hexa-coordinated species of H_4edta and H_4pdta.

EPR spectra of the polycrystalline complex $[Cu(pd3ap)]^{2-}$, recorded at 77 K, are shown in Fig. 6 (1). The spectrum is isotropic with a *g* value of 2.131. The broad and unresolved signal is due to the dipolar interaction which enlarges the spectral lines and obscures the hyperfine structure. The line width is 98.1 G. In solution the species with (2 N, 3 COO^-) coordination predominates from pH 4 to pH 11 with g_z 2.272, A_z 180.8×10^{-4} cm^{-1} (g_z/A_z 126). If these parameters are compared with those of the hexa-coordinated complex of H_4pdta with (2 N, 4 COO^-) coordination (H_4pdta forms the same (5,6,5) rings in the equatorial plane), a decrease of g_z and an increase of A_z can be observed; this change confirms the absence of a COO^- group in one of the two axial positions. The spectrum ($g_z > g_x \sim g_y$) indicates a tetragonal symmetry with the unpaired electron in the d_{x2-y2} orbital and a distorted square pyramidal geometry [36]. Therefore, the penta-coordinated structure of $[Cu(pd3ap)]^{2-}$ in the solid state is observed also in water, even if in this solvent the geometry can be described as intermediate between the square pyramid and the trigonal bipyramid rather than close to the TBP limit (see Fig. 2); probably, solid state effects not operating in solution stabilize the structure of 1.

EPR spectra of the polycrystalline complex $[Cu(pddadp)]^{2-}$ were recorded at 77 K (Fig. 6 (3)). Three broad and one sharp signal are detected in the region 2900–3400 G. The resonances at *g* = 2.214, 2.052 and 2.022 can be attributed to a Cu(II) in an octahedral geometry with a rhombic symmetry, for which a spectrum with three *g* values is expected [36,37]; the order $g_z \gg g_y > g_x > g_e$ indicates that the ground state is based mainly on the d_{x2-y2} orbital [36–38]. The resonance at *g* = 2.078 is characterized by a very small linewidth (2.4 Gauss). The most plausible assignment is to a double quantum (DQ) transition that involves the rapid consecutive absorption of two single quanta. The basis for this attribution are: (i) the phase of the resonance is compatible with that of the single quantum transitions; (ii) the *g* factor (2.078) is close to the average of the three *g* values of the single quantum transitions (2.096); (iii) the absorption cannot be simulated using only single quantum transitions and (iv) the line width of the band (2.4 Gauss) is significantly less than those measured for the single quantum transitions (>50 Gauss) [39]. These transitions have been detected for Fe(II) [40], Mn(II) [41], Ni(II) [42], Cu(II) [43,44] and suggest a strong interaction in the solid state between two neighboring Cu (II) ions to give a spin state *S* = 1. When $[Cu(pddadp)]^{2-}$ is dissolved in water, the hexa-coordinated species with (2 N, 4 COO^-) coordination (g_z 2.265, A_z 176.4×10^{-4} cm^{-1}, **I** in Fig. 6 (4)) is observed at pH > 5. EPR spectrum of the polycrystalline complex $[Cu(pdtp)]^{2-}$ was recorded at 77 K (Fig. 7 (1)). The spectrum is isotropic with a *g* value of 2.146. The broad absorption is due to the dipolar interaction in this case too. For H_4pdtp the species with (2 N, 3 COO^-) coordination is observed around neutral pH (I in Fig. 7 (2)), whereas that with (2 N, 4 COO^-) coordination (analogous to the solid state compound) is revealed at pH > 9 (II in Fig. 7 (2)) and coexists with the first one (indeed, the spectral resonances become large and little unresolved). This indicates that when all the chelate rings are six-membered the complexes are less stable. In conclusion, in aqueous solution H_4edta and its derivatives forms Cu(II) species with different coordination modes: hexa-coordination is favored when the two axial donors close five-membered chelate rings (H_4edta, H_4pdta). When the size of the axial chelate rings increases the hexa-coordinated coordination is less stable and higher pH values are necessary to observe (2 N, 4 COO^-) coordination. Comparing the X-ray crystal structures of 1 and 2 with the EPR spectra recorded in water, we found that the penta- and hexa-coordination occur also in solution.

3.3.1.1. IR data. The complexes have been further analyzed by means of IR and UV–Vis spectra (see Table and Figs. S4 in the Supporting information). The IR data (carboxylate region) are in agreement with the structures and molecular symmetries. As was found in the metal aminocarboxylic acid complexes [45,46], in the asymmetric carboxyl stretching region, the frequency assigned to five-membered rings [45] lies at higher energy than the corresponding frequency of six-membered chelate rings [46]. These complexes with C_1 and C_2 symmetry evidence two strong and separated bands in the asymmetric stretching carboxylate region (≈1640 cm^{-1} = higher energy of five-membered ring and ≈1570 cm^{-1} = lower energy of six-membered ring). Bands at 1630 cm^{-1} and 1564 cm^{-1} correspond to *trans*(O_6)-$[Cu(pddadp)]^{2-}$. Accordingly, the asymmetric stretching vibration of the five-membered glycinate rings, in case of $[Cu(pdta)]^{2-}$ [10], was at 1601 cm^{-1}. The same vibrations of $[Cu(pd3ap)]^{2-}$ complex are in accordance with a presence of three acetate rings and one propionate ring: 1622 cm^{-1} corresponds to the glycinate rings and 1559 cm^{-1} corresponds to the β-alaninato ring. As expected in $[Cu(pdtp)]^{2-}$ complex there is only one strong band at 1575 cm^{-1} originating from four carboxylate six-membered rings.

3.3.2. Computational experiments

Here we compared four DFT methods, LDA, BP86, B1LYP and B3LYP using the diverse basis sets in order to see structural and

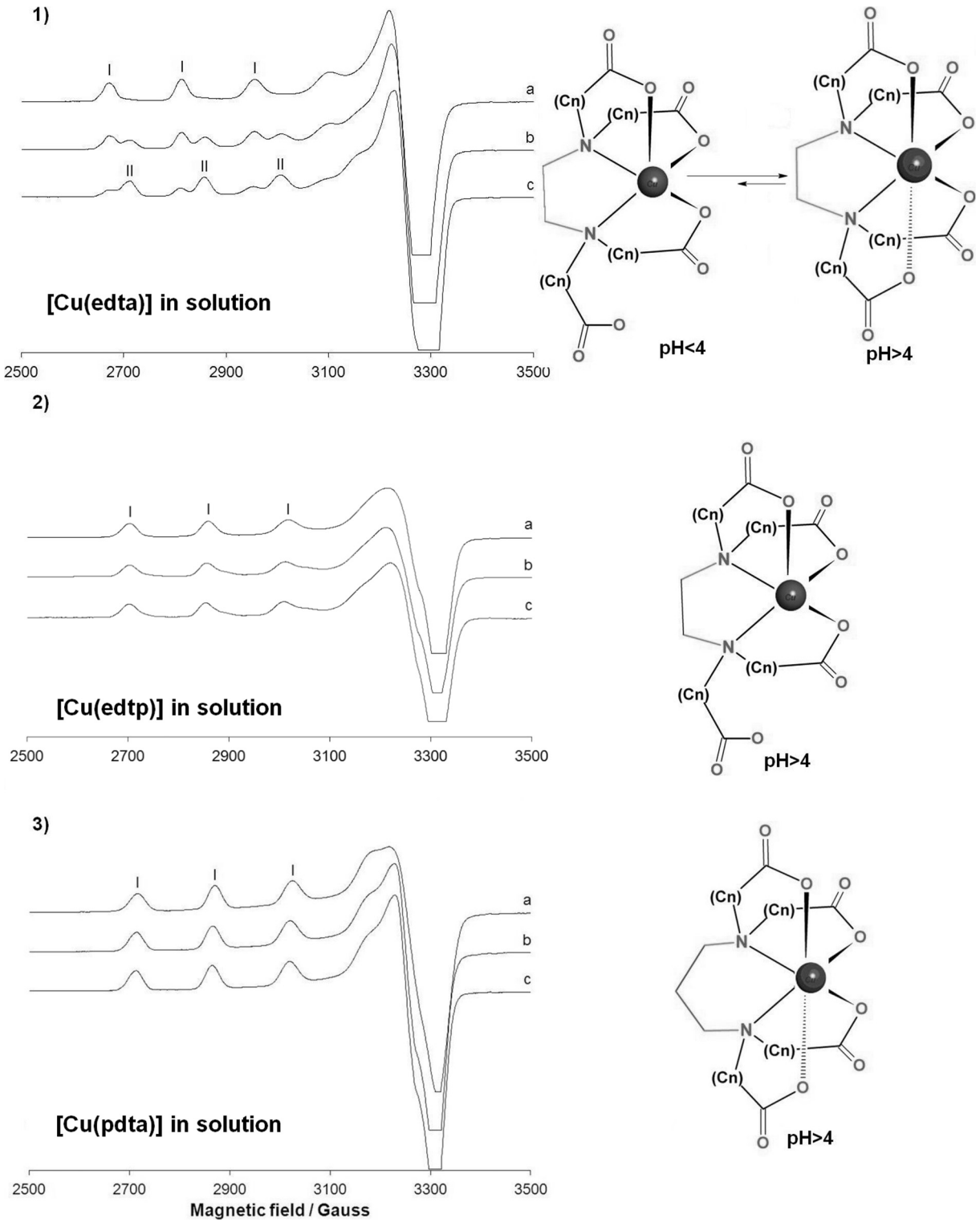

Fig. 5. (1) X-band anisotropic EPR spectra (120 K) recorded on a solution obtained dissolving Ba[Cu(edta)] in water (Cu^{II} concentration 1 mM): (a) pH 3.30; (b) pH 4.15 (spontaneous pH) and (c) pH 10.45; with **I** and **II** the first parallel resonances of the species with (2 N, 3 COO^-) and (2 N, 4 COO^-) coordination are indicated. (2) X-band anisotropic EPR spectra (120 K) recorded on a solution obtained dissolving K_2[Cu(edtp)] in water (Cu^{II} concentration 1 mM): (a) pH 3.60; (b) pH 6.10 (spontaneous pH); (c) pH 8.00. With **I** the first parallel resonances of the species with (2 N, 3 COO^-) coordination are indicated. (3) X-band anisotropic EPR spectra (120 K) recorded on a solution obtained dissolving Ba[Cu(pdta)] in water (Cu^{II} concentration 1 mM): (a) pH 3.35; (b) pH 5.30 (spontaneous pH) and (c) pH 9.75. With **I** the first parallel resonances of the species with (2 N, 4 COO^-) coordination are indicated.

energetic differences. Table 3 gives an overview of the energy differences for all isomers of $[Cu(pddadp)]^{2-}$ via three methods (LDA, BP86 and B1LYP) and the relative conformational energies derived from LFMM calculations using the force field developed previously. Table S5 (Supporting information) compares the theoretical and experimental structural parameters along with RMSD values between computed and X-ray determined structures for the P-APC series.

Table 2
EPR parameters of Cu(II) complexes formed with APCs.[a]

Ligand	g_z	A_z	g_z/A_z	Coordination mode
edta	2.330	154.6	151	2 N, 3 COO^-
edta	2.292	160.5	143	2 N, 4 COO^-
pdta	2.283	165.1	138	2 N, 4 COO^-
edtp	2.287	168.5	136	2 N, 3 COO^-
pd3ap	2.272	180.8	126	2 N, 3 COO^-
pddadp	2.265	176.4	128	2 N, 4 COO
pdtp	2.307	181.3	127	2 N, 3 COO^-
pdtp	~2.26	~175	~130	2 N, 4 COO

[a] Values of A_z reported in 10^{-4} cm^{-1}.

In general, the comparison between the theory and experiment is reasonably good. The DFT energies of $[Cu(1,3\text{-pddadp})]^{2-}$ isomers are in agreement with predictions based on the geometry of isolated *trans*(O_6) isomers (Table 3). The DFT results indicate that the crystallographic structure corresponds to the DFT lowest-energy structure regardless of the type of method or basis set. It can be observed from Table S5 that BP86/TZ2P and B1LYP/6-311++g(d,p) methods give the lower energy differences. The prediction that the *trans*(O_6) isomer has the lowest energy is consistent with the spectral results and our expectations from working with such systems. However, BP86 performs less well for structures (Table S5). In contrast, the LDA functional shows Cu–L distances very close to those observed in the solid state. One may see that RMSD value (Table S5 Supporting information) for equatorial atoms is four time lower than heavy atoms of whole molecule. This is again indication that carboxylate rings out of plane more distort from DFT calculated due to environmental impact (counter-ions, solid state, solvent) and that simple DFT job cannot solve this issue. The LFMM optimized, hexadentate $[Cu(pdta)]^{2-}$ and $[Cu(pdtp)]^{2-}$ complexes have shown usual axial and equatorial Cu–O and equatorial Cu–N distances. Thus a reasonable agreement between the X-ray and LFMM structure were obtained (Fig. 8).

The higher the number of six-membered chelate rings, the greater is the strain in the complex. This comes out of the structural strain analysis and can also be correlated with LFMM computed strain energies. For example, if the copper is removed from the complex, the strain energy for the tetraanionic ligand in its bound conformation can be computed. The ligand is then relaxed to its lowest energy conformation via a low mode molecular dynamics search. The greater the decrease in energy, the greater was the strain induced in the ligand upon binding to the metal center. The energy changes for H_4edta, H_4pddadp and H_4pdtp are 107, 136 and 180 kcal mol^{-1} respectively. As expected, the H_4pdtp ligand is the most strained and the associated complex is predicted to be less stable (LFMM bond average lengths are: Cu–O axial of 2.477 Å, Cu–O equatorial of 1.964 Å, and Cu–N of 2.133 Å).

TD-DFT and UV_Vis data Typical electronic absorption spectra of the octahedral $[Cu(P\text{-APC})]^{2-}$ complex is shown in Fig. 9. One can see that whole spectral range can be divided into two parts: UV and Vis/Near_IR regions. Regarding to the shape of spectra the major (energy and absorptivity) region belongs to UV range. Appearance of one sharp band is common for all the P-APC complexes. Energy position of these bands is not substantially different too, found within the range of 2–5 nm. This region was not, evidently, within scope of our interest. The most important one is a visible region reflecting usually geometry configuration and ligand field strength (LFS) in relation of copper(II) complexes. The Near_IR region is occasionally characterized by one weak band of low absorbance which is rarely detected being covered by the higher intensity bands (see Fig. 9). All of the complexes are blue and experimentally exhibit one asymmetric absorption band irrespective of the underlying approximate C_1 or C_2 symmetry.

If we look at Table 4, the highest visible absorption band was obtained for the *trans(O$_6$)*-$[Cu(pddadp)]^{2-}$ complex (658 nm) and the lowest for the $[Cu(pdtp)]^{2-}$ complex (752 nm). It was observed that in the absence of glycinato rings in the axial position the band of complexes with a higher number of glycine chains in the

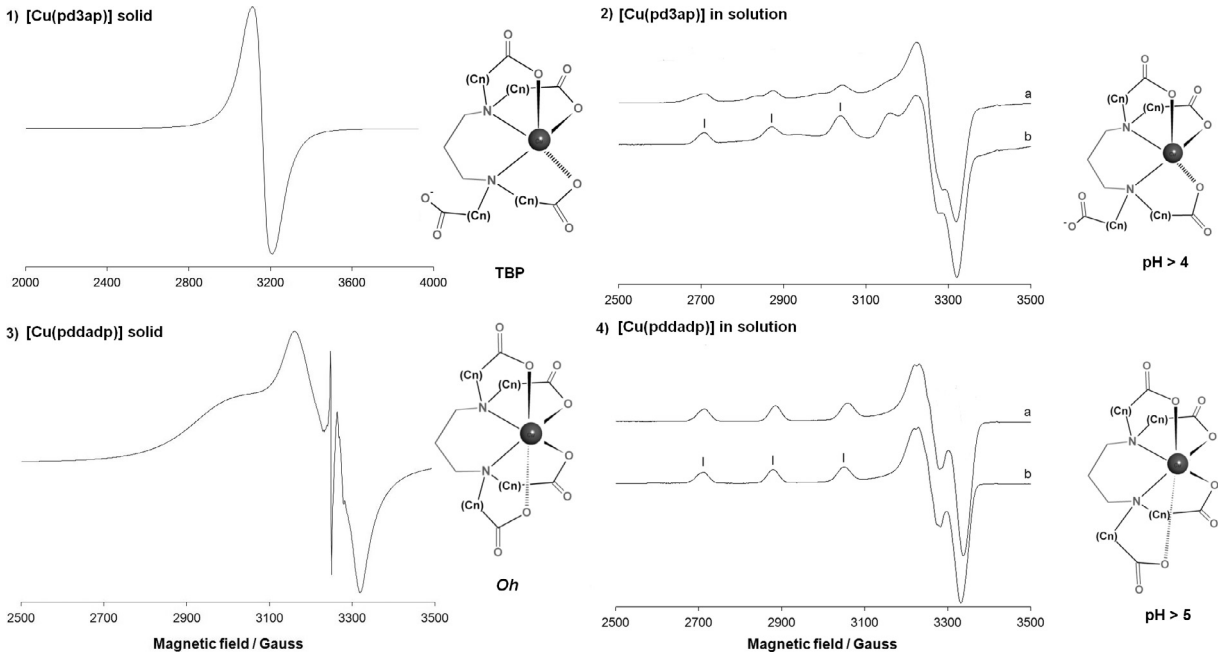

Fig. 6. (1) X-band EPR spectra of the polycrystalline complex Ba[Cu(pd3ap)] recorded at 77 K. (2) X-band anisotropic EPR spectra (120 K) recorded on a solution obtained dissolving Ba[Cu(pd3ap)] in water (Cu^{II} concentration 1 mM): (a) pH 5.90 (spontaneous pH) and (b) pH 10.45; with **I** the first parallel resonances of the species with (2 N, 3 COO^-) coordination are indicated. (3) X-band EPR spectra of the polycrystalline complex Ba[Cu(pddadp)] recorded at 77 K. (4) X-band anisotropic EPR spectra (120 K) recorded on a solution obtained dissolving Ba[Cu(pddadp)] in water (Cu^{II} concentration 1 mM): (a) pH 5.80 (spontaneous pH) and (b) pH 9.10–10.70; with **I** the first parallel resonances of the species with (2 N, 4 COO^-) coordination are indicated.

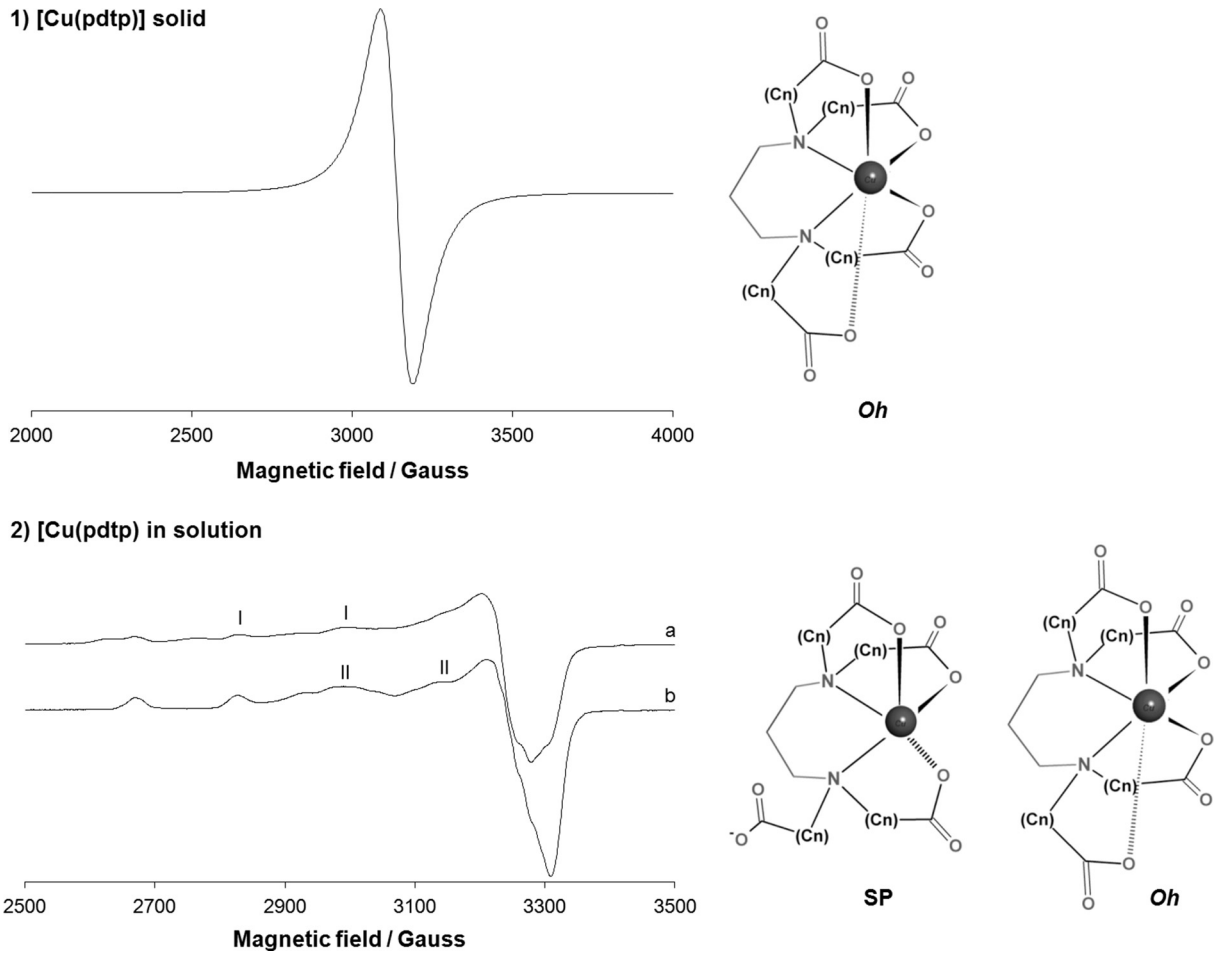

Fig. 7. (1) X-band EPR spectra of the polycrystalline complex Ba[Cu(1,3-pdtp)] recorded at 77 K; (2) X-band anisotropic EPR spectra (120 K) recorded on a solution obtained dissolving Ba[Cu(1,3-pdtp)] in water (Cu^{II} concentration 1 mM): (a) pH 3.50; (b) pH 4.05; (c) pH 7.05 (spontaneous pH) and (d) pH 9.50. With **I**, **II** and **III** the first parallel resonances of the species with only one amine nitrogen bound to Cu(II) (**I** and **II**) and with (2 N, 2 COO^-) coordination (**III**) are indicated.

Table 3
Comparison of the relative energy data for $[Cu(pddadp)]^{2-}$ isomers calculated by DFT and LFMM.

Isomer	LDA/DZP	BP86/DZP	BP86/TZP	BP86/TZ2P	B1LYP/6-311++g(d,p)	LFMM
trans(O_6)[a]	0	0	0	0	0	0
trans(O_5O_6)	3.6	2.4	2.5	1.9	1.74	0.2
trans(O_5)	8.7	6.1	5.6	5.3	4.93	1.1

[a] The isomer with the lowest-energy minimum has been indicated with 0 kcal mol^{-1}.

equatorial plane is shifted toward higher energy. Accordingly, it is expected that $[Cu(pdtp)]^{2-}$ without any glycine ring shows the lowest energy band. The other two complexes $[Cu(1,3\text{-}pd3ap)]^{2-}$ and $[Cu(pdtp)]^{2-}$ show single asymmetrical absorption bands associated with shoulders, especially in the case of the $[Cu(pd3ap)]^{2-}$ complex (see spectrum in Supporting information S6). It is documented for copper(II) complexes that a single visible band with a high-energy shoulder is indicative of a trigonal bipyramidal stereochemistry while an absorption envelope with a low-energy shoulder is characteristic of a square pyramidal geometry [47]. The complex $[Cu(pd3ap)]^{2-}$ shows a visible band with an obvious shoulder on the higher energy side which is according to the above findings consistent with trigonal bipyramidal (TBP) geometry and X-ray structure reported in this work.

As an example of TD-DFT transitions we are giving here the full simulated UV–Vis spectra of $[Cu(pdta)]^{2-}$ complex ion (Fig. 9). The molecular orbital analysis of TD-DFT data shows that the main UV transitions are due to ligand to metal charge transfers (LMCT). Within the visible region TD-DFT gave three transitions: one at higher energy and higher oscillator strength followed by the two additional transitions of much lower intensity. The most intense transition generally determines position of convoluted band as well. This excitation line is a consequence of d-d transition mix: 27% HOMO−20 → LUMO and 23% HOMO−21 → LUMO. The near IR region is occasionally characterized by one excitation line of low oscillator strength which is covered by the 63% of HOMO → LUMO transition (see Fig. 9). The ground state in all the cases is $d_{x2\text{-}y2}$ and the main percentage contribution of orbitals involved in singlet transition is attributed to d_{z2}, d_{xy}, d_{xz} and d_{yz} orbitals (see Supporting information S7).

Several strategies have been proposed to extract, using quantum-mechanic, excited state information from the ground state density. The most promising of which is time-dependent TD-DFT designed by Runge and Gross [48]. TD-DFT calculates the frequency-dependent linear response of the charge density with respect to a time-dependent perturbation in the electric field

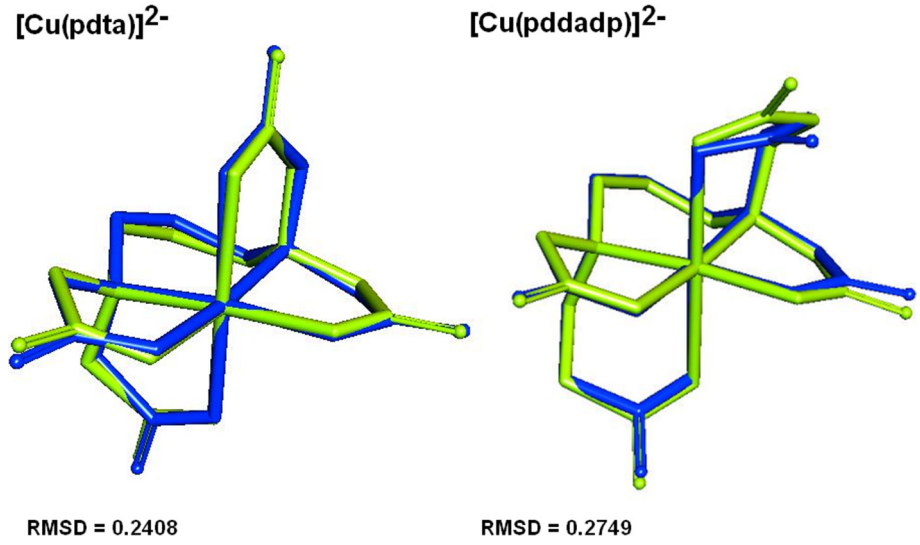

Fig. 8. Overlay of LFMM (yellow) and X-ray (blue) calculated structures. (Color online).

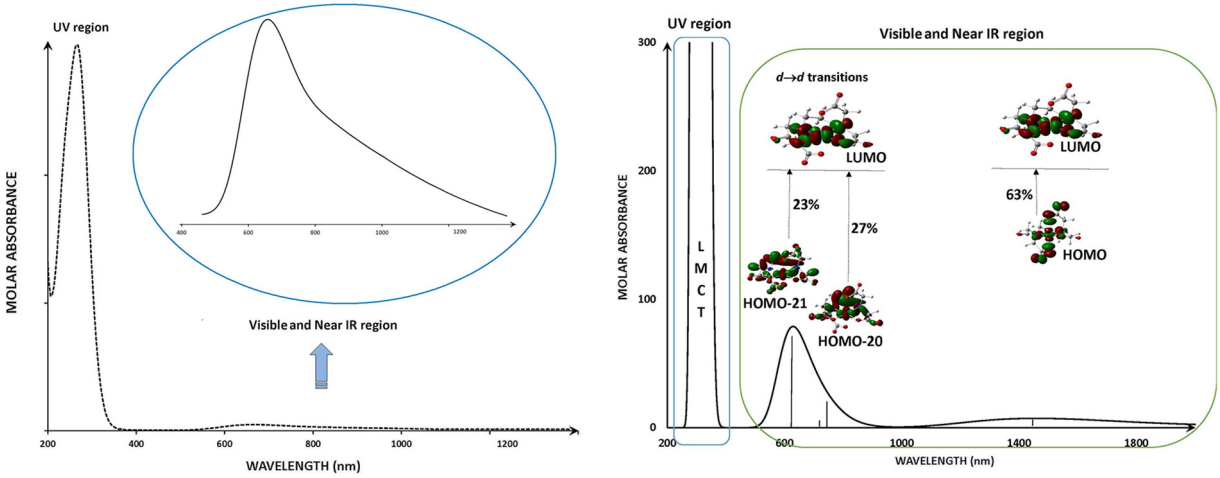

Fig. 9. Left: UV–Vis spectrum of $[Cu(pddadp)]^{2-}$ obtained from water solution under pH ~7; right: principal MO transitions within Vis_Near_IR region in case of $[Cu(pdta)]^{2-}$ ion.

Table 4
TD-DFT and experimental Absorption data in water for hexadentate Cu(II)–P-APCs complexes.

Complex	Absorption[1]	TD-DFT[2]						Ref.
		B1LYP		B3LYP		BP86		
	λ (nm)/ε (mol^{-1} dm^3 cm^{-1})	λ/ε	*Esf*[3]	λ/ε	*Esf*	λ/ε	*Esf*	
$[Cu(pdta)]^{2-}$	704/84	640/80	1.100	613/78	1.148	535/3325	1.318	[10], This work
$[Cu(pddadp)]^{2-}$	658/68	613 /68	1.073	592/86	1.111	590/2130	1.115	This work
$[Cu(pdtp)]^{2-}$	752/106	690/112	1.089	654/186	1.150	578/3140	1.301	This work
$[Cu(pd3ap)]^{2-}$,[4]	680 sh838/69	917/7401020/ 416 (sh)	0.914	909/9851010/ 557 (sh)	0.922	905/28801020/ 1490 (sh)	0.926	This work
[Cu(pda3p)]$^{2-}$,[5]	*715/90 predicted*	*655/90*	*1.090*					This work

Italic refers to complex has not been experimentally isolated.
[1] Absorption spectra were recorded under pH ~ 7.
[2] Simulated UV–Vis absorption band (visible or near IR region) from Gaussian TD-DFT calculations. The half-bandwidths, $\Delta_{1/2,I}$, were taken to be equal to 3000 cm^{-1}.
[3] Energy scaling factor.
[4] TBP complex.
[5] Simulated and predicted absorption visible peak position of not synthetized *trans*(O_6)-$[Cu(pda3p)]^{2-}$ complex anion.

[49]. The results include calculation of excitation energies ω_I and oscillator strengths f_I for transition between the ground and excited states I of a system [50]. The difficulties associated with the calculation of excited states were overcome describing these excitations in terms of ground state properties such as molecular orbital (MO) contributions.

Holland and Green compared the performance of 41 different XC functionals in their ability to predict the UV–Vis spectra of copper and zinc bis(thiosemicarbazonato) complexes [51]. Hybrid DFT methods were found to outperform all pure DFT functionals. Of the functionals tested, B1LYP gave the most accurate results regarding to the all parameters monitored for the copper com-

plexes [51]. Starting from their results we performed time-dependent Density Functional Theory calculations using optimized geometries of our complexes at the three different methods, namely BP86, B1LYP and B3LYP; we used the same basis set 6-311++G(d,p), as Holland and Green, in order to further check the viability of TD-DFT results in our case. In each case, oscillator strengths and excitation energies for transition between the ground state and the first 10 excited stated states were calculated. We have used the AOMix program [23] to produce Gaussian simulated UV–Vis spectra based on the TD-DFT calculations. Each calculated transition between the ground and excited states I, can be modeled by a single Gaussian function in accordance with Eq. (1).

$$\varepsilon(\omega) = 2.174 \times 10^{8} \sum_{I} \frac{f_I}{\Delta_{\frac{1}{2},I}} \exp\left(-2.773 \frac{(\omega - \omega_I)^2}{\Delta^2_{\frac{1}{2},I}}\right) \quad (1)$$

$$\sum_{I} f(I) = 4.319 \times 10^{-9} \int \varepsilon(\omega) d(\omega) \quad (2)$$

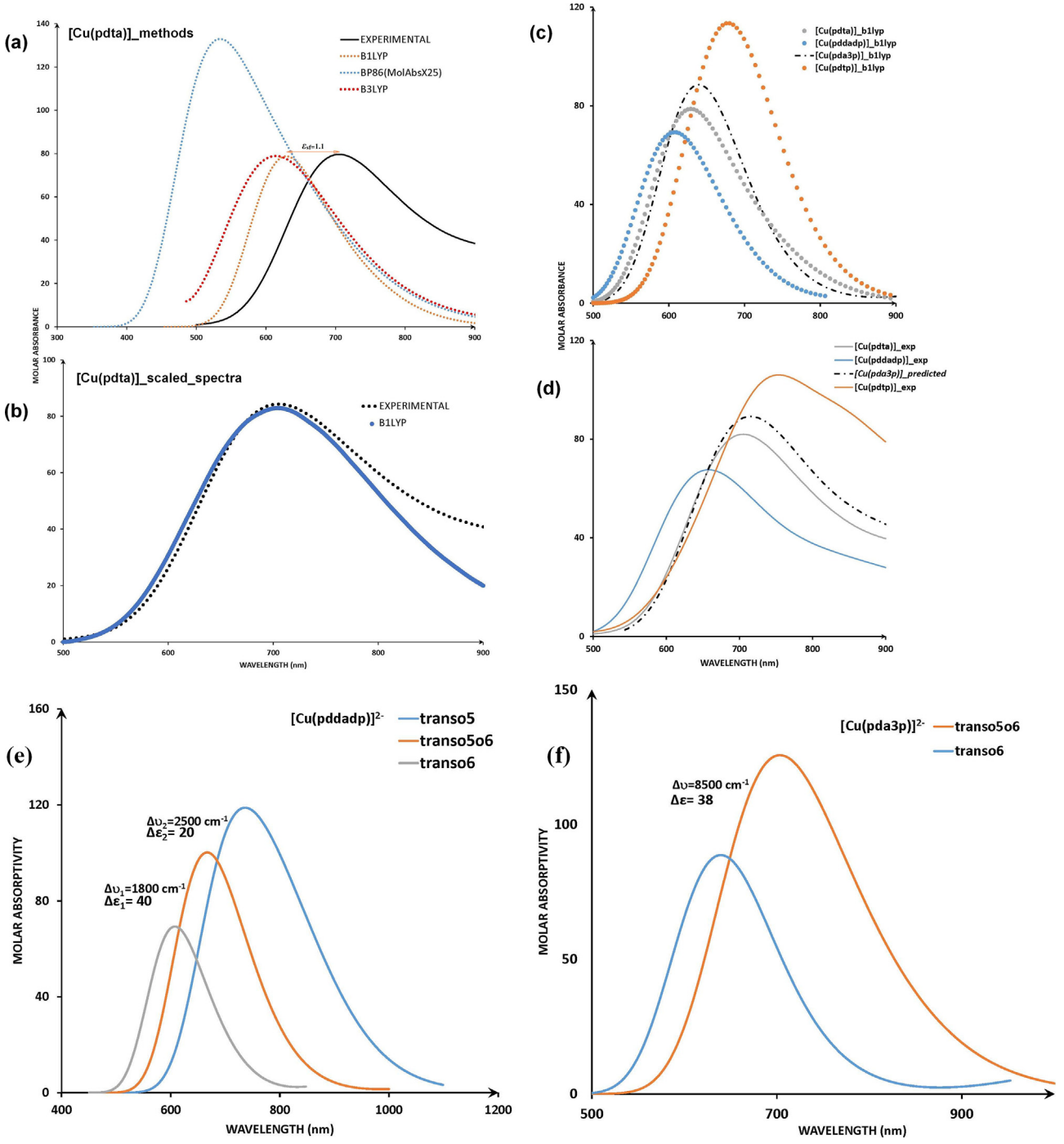

Fig. 10. (a) Gaussian shapes of TD-DFT data for $[Cu(pdta)]^{2-}$ ion calculated by different methods; (b) overlay of convoluted B1LYP data and experimental spectrum of $[Cu(pdta)]^{2-}$ ion; (c) B1LYP and (d) experimental band (visible region) of octahedral $[Cu(pdta\text{-type})]^{2-}$ complexes; TD-DFT data calculated for different isomers of (e) $[Cu(pddadp)]^{2-}$ ion and (f) $Cu(pda3p)]^{2-}$ ion.

where ε stands for molar absorptivity (molar absorption coefficient), ω_I stands for TD-DFT calculated excitation energies, (in cm^{-1}), f_I is transition oscillator strength (dimensionless), and $\Delta_{1/2,I}$ stands for half-band width, (in cm^{-1}). The total integrated intensity under the absorption profile is equal to the sum of the oscillator strengths and is given by Eq. (2). We have changed half- band width only during spectra convolution. Gaussian convoluted TD-DFT data are compared with experimental values as well (see Table 4 and Fig. 10). For low resolution spectroscopy, Gaussian functions have been shown to be suitable for accurate simulation of experimental band shapes [52]. Experimental half-band widths are generally unknown, and are difficult to estimate due to their high dependence on solvation and/or vibronic coupling within the system. After we used different values for this parameter during convolution process to minimize the difference between the experimental and simulated UV–Vis spectra, the AOMix default value of 3000 cm^{-1} has been taken as a common value in all the cases. Calculated energies are often scaled, particularly in vibrational frequency analysis. Therefore, an energy scaling factor, E_{SF}, was also applied after each simulation. It is evident from Table 4 and Fig. 10(a and b), that our results are in agreement with conclusions of Holland and Green [51]. The parameters of particular importance are band energy position along with its ε value and E_{SF}. In other words, B1LYP and B3LYP are far more accurate methods than BP86. Furthermore B1LYP appear to be method of choice for calculating TD-DFT data for copper(II) aminopolycarboxylate complexes not only because of well fitted band shapes and energies but also because of very comparable molar absorption coefficients with experimental ε data (see Table 4, Fig. 10(c and d)). Resemblance of the mutual band positions and their shapes with experimental spectra (Fig. 10(c and d)) is more than obvious. We have to say that the higher ε value on the low energy side of each band is just a consequence of already mentioned environmental influence (solvent, counter-ion, ...) and/or vibronic coupling within the system.

In addition, we are going to demonstrate here on how visible spectra of unknown compound can be predicted using the procedure described here. For this purpose we took not yet prepared $[Cu(pda3p)]^{2-}$ complex ion (pda3p stands for 1,3-propanediamine-*N*-acetato-*N*,*N*′,*N*′-3-tripropionato tetraanion). Theoretically this ligand may give us two different geometrical isomers: *trans* (O_6) and *trans*(O_5O_6) (Fig. 1). We modeled these isomers by the LFMM conformational analysis and took the less strained molecules. Then we optimized molecules at the B1LYP/6-311++G(d,p) level. It was shown that the *trans*(O_6) isomer is more stable for ~4 kcal/mol. The TD-DFT has been calculated and data convoluted using same level of theory and convolution procedure for both isomers. The visible spectra of the most stable *trans*(O_6) isomer is placed in Fig. 10(c and d) along with spectra reported in this work. Furthermore, we may see the difference between simulated spectra of different isomers of $[Cu(pddadp)]^{2-}$ and $[Cu(pda3p)]^{2-}$ complexes (Fig. 10(e and f)). It is symptomatic that the most stable complexes tend to have their spectra with lower molar absorptivity. This is sensible taking into account that we expected lower absorptivity for the less strained system holding less rigid 1,3-propanediamine backbone ring. Therefore, the energy difference and molar absorptivity difference (Fig. 10) in case of different isomers are enough evidenced in order to differentiate each one by working with them in practice.

4. Conclusions

We wish to stress out several important points that arise from above discussion:

- P-APC chelates act as hexadentates or pentadentates toward Cu (II) ion depending on number of six-membered rings and pH of water solution. This fact is well confirmed by their EPR and UV–Vis spectra and solid state structures.
- The symmetric chelates with mixed carboxylate chains (H_4eddadp and $H_4$1,3-pddadp) serve better for octahedral coordination of copper ion. In this way they significantly reduce the possibility of formation of ternary complexes. This property along with high $[CuL]^{2-}$ stability constants make them a good candidates for selective chelating drugs against excess of copper found either in cell's cytoplasm or blood plasma of living organisms.
- Spectral results are indicative for the penta or hexa-coordination of APC ligands toward copper(II) ion in aqueous solution. However, other Cu(II) species with different protonation degree may occur as a function of pH. From the EPR results we may further evaluate a hexa-coordinated structure as a favored one when the two axial COO^- donors of APC ligands close five-membered chelate rings around copper(II) ion.
- It could be underline that different cations may influence different behavior of complexes formed. That means the presence of divalent cations (Ba^{2+} but, we believe, Mg^{2+} and Ca^{2+} as well) leads to the formation of more distorted $[CuL]^{2-}$ species the opposite of monovalent cations (Na^+ or K^+) which tend more toward the regular form.
- Vis_Near_IR and EPR curves of $[CuL]^{n-}$ species are their characteristic properties and can be used to identify the various types of complexes for particular chelate case: penta- or hexa-coordinated; trigonal–bipyramidal or octahedral; different isomers – different spectral properties. Absorption spectra of complexes and their isomers can be easily modeled and predicted by use of computational chemistry (TD-DFT). This in turn would make us possible to monitor the modeling biological reactions describing chelate-copper-substrate system.

Acknowledgements

The authors are grateful to the Serbian Ministry of Education and Science for financial support (Project III41010). RJD acknowledges the support of Chemical Computing Group and access to the Molecular Operating System software.

Appendix A. Supplementary data

CCDC 1054491 and 1054492 contains the supplementary crystallographic data for complexes **1** and **2**. These data can be obtained free of charge via http://www.ccdc.cam.ac.uk/conts/retrieving.html, or from the Cambridge Crystallographic Data Centre, 12 Union Road, Cambridge CB2 1EZ, UK; fax: (+44) 1223-336-033; or e-mail: deposit@ccdc.cam.ac.uk. Supplementary data associated with this article can be found, in the online version, at http://dx.doi.org/10.1016/j.poly.2016.12.025.

References

[1] S.J.S. Flora, V. Pachauri, Int. J. Environ. Res. Public Health 7 (2010) 2745.
[2] J.J. Anzinger, I. Mezo, X. Ji, A.M. Gabali, L.L. Thomas, G.T. Spear, Virus Res. 122 (2006) 183.
[3] A.C. Chang, K. Kumar, M.F. Tweedle, Dual functioning excipient for metal chelate contrast agents, U.S. Patent, 7,385,041, June 10, 2008.
[4] M. Blanuša, V.M. Varnai, M. Piasek, K. Kostial, Curr. Med. Chem. 12 (2005) 2771.
[5] Z.D. Matović, V.D. Miletić, M. Ćendić, A. Meetsma, P.J. van Koningsbruggen, R.J. Deeth, Inorg. Chem. 52 (2013) 1238.
[6] M. Ćendić, Z.D. Matović, R.J. Deeth, J. Comp. Chem. 34 (2013) 2687.
[7] R.C. Courtney, S. Chaberek, A. Martell, J. Am. Chem. Soc. 75 (1953) 4814.
[8] P. Djurdjević, D. Radanović, M. Cvijović, M. Dimitrijević, D. Veselinović, Polyhedron 11 (1992) 197.

[9] S. Kaizaki, M. Byakuno, M. Hayashi, J.I. Legg, K. Umakoshi, S. Ooi, Inorg. Chem. 26 (1987) 2395.
[10] U. Rychlewska, D.D. Radanović, V.S. Jevtović, D.J. Radanović, Polyhedron 19 (2000) 1.
[11] MOE Molecular Operating Environment, 2011.10, Chemical Computing Group, Montreal, Canada, 2011.
[12] I.N. Polyakova, A.L. Poznyak, V.S. Sergienko, Crystallogr. Rep. 45 (2000) 41.
[13] U. Rychlewska, D.D. Radanović, M.Đ. Dimitrijević, D.M. Ristanović, M.M. Vasojević, D.J. Radanović, Polyhedron 20 (2001) 2523.
[14] D.J. Radanović, B.V. Prelesnik, D.D. Radanović, Z.D. Matović, B.E. Douglas, Inorg. Chim. Acta 262 (1997) 203.
[15] Bruker, SMART, SAINT, SADABS, XPREP and SHELXTL/NT Area Detector Control and Integration Software. Smart Apex Software Reference Manuals, Bruker Analytical X-ray Instruments Inc., Madison, WI, USA, 2000.
[16] P.T. Beurskens, G. Beurskens, R. de Gelder, S. García-Granda, R.O. Gould, R. Israël, J.M.M. Smits, The DIRDIF-99 Program System, Crystallography Laboratory, University of Nijmengen, Nijmengen, The Netherlands, 1999.
[17] G. te Velde, F.M. Bickelhaupt, S.J. van Gisbergen, C. Fonseca Guerra, E.J. Baerends, J.G. Snijders, T.J. Ziegler, Comput. Chem. 22 (2001) 931.
[18] C. Fonseca Guerra, J.G. Snijders, G. te Velde, E.J. Baerends, Theor. Chem. Acc. 99 (1998) 391.
[19] ADF2007.01; SCM, Theoretical Chemistry, Vrije Universiteit: Amsterdam, The Netherlands, http://www.scm.com.
[20] M.J. Frisch, G.W. Trucks, H.B. Schlegel, G.E. Scuseria, M.A. Robb, J.R. Cheeseman, G. Scalmani, V. Barone, B. Mennucci, G.A. Petersson, H. Nakatsuji, M. Caricato, X. Li, H.P. Hratchian, A.F. Izmaylov, J. Bloino, G. Zheng, J.L. Sonnenberg, M. Hada, M. Ehara, K. Toyota, R. Fukuda, J. Hasegawa, M. Ishida, T. Nakajima, Y. Honda, O. Kitao, H. Nakai, T. Vreven, J.A. Montgomery, J.E. Peralta, F. Ogliaro, M. Bearpark, J.J. Heyd, E. Brothers, K.N. Kudin, V.N. Staroverov, R. Kobayashi, J. Normand, K. Raghavachari, A. Rendell, J.C. Burant, S.S. Iyengar, J. Tomasi, M. Cossi, N. Rega, J.M. Millam, M. Klene, J.E. Knox, J.B. Cross, V. Bakken, C. Adamo, J. Jaramillo, R. Gomperts, R.E. Stratmann, O. Yazyev, A.J. Austin, R. Cammi, C. Pomelli, J.W. Ochterski, R.L. Martin, K. Morokuma, V.G. Zakrzewski, G.A. Voth, P. Salvador, J.J. Dannenberg, S. Dapprich, A.D. Daniels, Ö. Farkas, J.B. Foresman, J.V. Ortiz, J. Cioslowski, D.J. Fox, Gaussian 09, revision A.1, Gaussian Inc, Wallingford, CT, 2009, and references therein.
[21] F. Weigend, R. Ahlrichs, Phys. Chem. Chem. Phys. 7 (2005) 3297.
[22] a) V.A. Rassolov, J.A. Pople, M.A. Ratner, T.L. Windus, J. Chem. Phys. 109 (1998) 1223;
b) V.A. Rassolov, M. Ratner, J.A. Pople, P.C. Redfern, L.A. Curtiss, J. Comp. Chem. 22 (2001) 976.
[23] S.I. Gorelsky, AOMix: Program for Molecular Orbital Analysis, http://www.sg-chem.net/, version X.X, 2013.
[24] R.J. Deeth, N. Fey, B.J. Williams-Hubbard, J. Comput. Chem. 26 (2005) 123.
[25] R.J. Deeth, L.J.A. Hearnshaw, Dalton Trans. 22 (2005) 3638.
[26] N. Sakagami, S. Kaizaki, Dalton Trans. 2 (1992) 291.
[27] Z. Matović, A. Meetsma, V.D. Miletić, P.J. van Koningsbruggen, Inorg. Chim. Acta 360 (2007) 2420.
[28] A.W. Addison, T. Nageswara Rao, J. Reedijk, J. van Rijn, G.C. Verschoor, Dalton Trans. 7 (1984) 1349.
[29] A.A.G. Tomlinson, B.J. Hathaway, D.E. Billing, P. Nicholls, J. Chem. Soc. A (1969) 65.
[30] B.J. Hathaway, Compr. Coord. Chem., Pergamon, Oxford, 1987.
[31] B.J. Hathaway, P.G. Hodgson, J. Inorg. Nucl. Chem. 35 (1973) 4071.
[32] B.V. Prelesnik, D.D. Radanović, Z.D. Tomić, P.T. Djurdjević, D.J. Radanović, D.S. Veselinović, Polyhedron 15 (1996) 3761.
[33] G. Micera, D. Sanna, R. Dallocchio, A. Dessì, J. Coord. Chem. 25 (1992) 265.
[34] D. Sanna, C.G. Ágoston, G. Micera, I. Sóvágó, Polyhedron 20 (2001) 3079.
[35] H. Yokoi, A.W. Addison, Inorg. Chem. 16 (1977) 1341.
[36] E. Garribba, G. Micera, J. Chem. Educ. 83 (2006) 1229.
[37] B.J. Hathaway, D.E. Billing, Coord. Chem. Rev. 5 (1970) 143.
[38] A. Ray, C. Rizzoli, G. Pilet, C. Desplanches, E. Garribba, E. Rentschler, S. Mitra, Eur. J. Inorg. Chem. 20 (2009) 2915.
[39] J.R. Pilbrow, Transition Ion Electron Paramagnetic Resonance, Vol. 95, Clarendon Press, Oxford, 1990, pp. 1307.
[40] H. Kim, J. Lange, Phys. Rev. B 17 (1978) 4207.
[41] P.P. Sorokin, I.L. Gelles, W.V. Smith, Phys. Rev. 112 (1958) 1513.
[42] J.W. Orton, P. Auzins, J.H.E. Griffiths, J.E. Wertz, Proc. Phys. Soc. 78 (1961) 554.
[43] L.M.B. Napolitano, O.R. Nascimento, S. Cabaleiro, J. Castro, R. Calvo, Phys. Rev. B 77 (2008), 214423/1-214423/13.
[44] M. Perec, R. Baggio, R.P. Sartoris, R.C. Santana, O. Peña, R. Calvo, Inorg. Chem. 49 (2009) 695.
[45] K. Nakamoto, Y. Morimoto, A.E. Martell, J. Am. Chem. Soc. 83 (1961) 4528.
[46] M.B. Ćelap, S.R. Niketić, T.J. Janjić, V.N. Nikolić, Inorg. Chem. 6 (1967) 2063.
[47] D.-H. Lee, N.M. Narasimha, K.D. Karlin, Inorg. Chem. 36 (1997) 5785.
[48] E. Runge, E.K.U. Gross, Phys. Rev. Lett. 52 (1984) 997.
[49] W. Koch, M.C. Holthausen, A Chemist's Guide to Density Functional Theory, Wiley-VCH Verlag GmbH, Weinheim, Germany, 2001.
[50] C.A. Ullrich, J. Chem. Theory Comp. 5 (2009) 859.
[51] J.P. Holland, J.C. Green, J. Comput. Chem. 31 (2010) 1008.
[52] G.M. Pearl, M.C. Zerner, A. Broo, J. Mc Kelvey, J. Comp. Chem. 19 (1998) 781–796.